Tensor renormalization group study of hard-disk models on a triangular lattice

S. S. Akimenko,* V. A. Gorbunov, A. V. Myshlyavtsev, and P. V. Stishenko
Department of Chemical Engineering, Omsk State Technical University, Prospekt Mira 11, Omsk 644050, Russian Federation

(Received 25 April 2019; published 7 August 2019)

High accuracy and performance of the tensor renormalization group (TRG) method have been demonstrated for the model of hard disks on a triangular lattice. We considered a sequence of models with disk diameter ranging from a to $2\sqrt{3}a$, where a is the lattice constant. Practically, these models are good for approximate description of thermodynamics properties of molecular layers on crystal surfaces. Theoretically, it is interesting to analyze if and how this sequence converges to the continuous model of hard disks. The dependencies of the density and heat capacity on the chemical potential were calculated with TRG and transfer-matrix (TM) methods. We benchmarked accuracy and performance of the TRG method comparing it with TM method and with exact result for the model with nearest-neighbor exclusions (1NN). The TRG method demonstrates good convergence and turns out to be superior over TM with regard to considered models. Critical values of chemical potential (μ_c) have been computed for all models. For the model with next-nearest-neighbor exclusions (2NN) the TRG and TM produce consistent results ($\mu_c = 1.75587$ and $\mu_c = 1.75398$ correspondingly) that are also close to earlier Monte Carlo estimation by Zhang and Deng. We found that 3NN and 5NN models shows the first-order phase transition, with close values of μ_c ($\mu_c = 4.4488$ for 3NN and $4.4 < \mu_c < 4.5$ for 5NN). The 4NN model demonstrates continuous yet rapid phase transition with $2.65 < \mu_c < 2.7$.

DOI: 10.1103/PhysRevE.100.022108

I. INTRODUCTION

Theoretical investigations of two-dimensional (2D) condensed systems, such as adsorption layers, often rely on lattice models of various complexity [1–12]. Phase diagrams of complicated lattice models demonstrate a large number of phases with a large unit cell and narrow region of existence. Due to these features, an application of the traditional methods of statistical physics for studying such models usually face a number of predictable challenges [7,8,13–16]. Using the standard metropolis Monte Carlo method, it is difficult to achieve an equilibrium state, especially in the phase-transition regions due to the critical slowdown and degeneracy of phases. However, it is worth mentioning that advanced Monte Carlo techniques like cluster algorithms, expanded ensemble, and replica exchange methods can be rather efficient in locating the critical points and revealing the type and the universality of the phase transitions [17,18]. The transfer-matrix technique as well as cluster methods has serious limitations on the period of considered phases, since the requirements for computing power grow exponentially with the system size reaching prohibitive values in some cases [19]. On the other hand, the narrow region of the phases existence requires a high accuracy in determining their boundaries. For the reasons listed above, reliable thermodynamic analysis of the adsorption layers and analysis of their phase behavior is complicated.

Recently, the tensor renormalization group (TRG) method was formulated by Levin and Nave [20]. It overcomes the main limitation of the transfer-matrix method allowing us to investigate the systems of virtually infinite size. The main idea of the TRG method is close to the density matrix renormalization group method [21], which has shown high efficiency in the study of highly correlated quantum systems in one dimension. However, some challenges arose in generalization to higher dimensions. The TRG method is based on an iterative contraction of a tensor network with the subsequent singular value decomposition of the tensor and its reduction. Tensor network algorithms are especially effective for the strongly correlated systems and are widely used in the investigation of quantum models [22–24]. Various modifications of this approach with growing accuracy and performance regularly appear in literature [25–30].

In this paper, we investigated the capabilities of the TRG method for studying the thermodynamic of hard-core lattice models. These models qualitatively describe a behavior of adsorption layers with isotropic repulsion between adsorbed complexes. The relatively strong repulsions become prohibitive at a certain distance and low-enough temperatures. Thus, phase transitions in many adsorption systems in fact are extensions of phase transitions in hard-core models to finite-temperature range. We have considered the sequence of hard-disks models with different sizes. This set of models is interesting because the discreteness of the disk position on the surface decreases with increasing the disk size and, in the limit of infinitely large disk, a transition to the continuous model is expected. As an example, we refer to the porphyrins adsorption on the gold surface [31–33]. Structure of the resulting dense phase is determined only by geometry of the adsorbed molecules and the interactions between them. To a certain extent, this sequence is a transition from the Langmuir adsorption lattice model to continuous models of hard segments (Volmer model) or hard disks.

*akimenkosergey@mail.ru

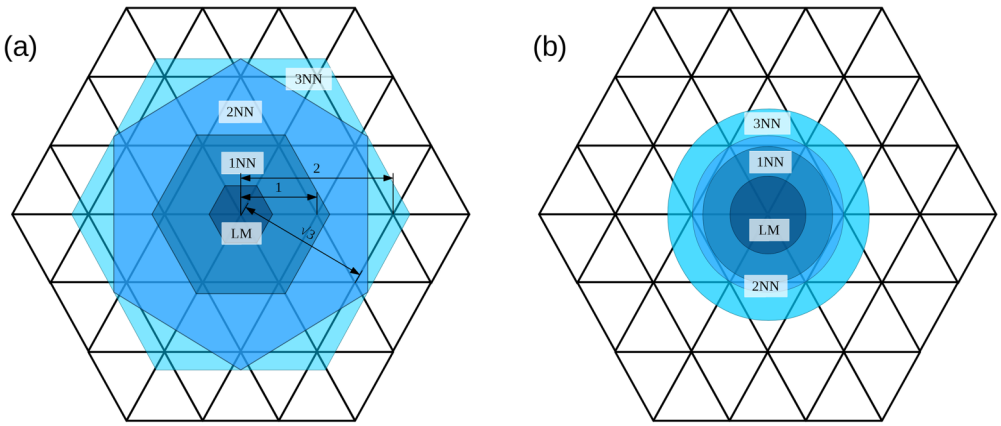

FIG. 1. Schematic representation of the studied models: (a) The sequence of the neighbor exclusions and (b) corresponding sequence of hard disks.

It turned out that this sequence of models exhibit two types of phase transitions—continuous and discontinuous ones. Similar behavior was earlier observed for square lattice [8]. Thereby we took the opportunity to benchmark performance and accuracy of the novel TRG method against proven hard tasks—detection of phase transition type and calculation of critical parameters for both continuous and discontinuous transitions.

II. MODELS

Here we describe the considered sequence of models on a triangular lattice. Models of hard disks on square lattice has been investigated in numerous studies [7,8,13,14,34–37] and remarkable nonobvious features of phase behavior have been revealed. In contrast, the same models on triangular lattice are much less studied [15,16,38]. Most likely it is due to higher complexity of calculations in that case. Besides theoretical interest, triangular lattice is a model of many practically important surfaces: Pt(111), Au(111), Cu(111), Zn(0001), etc.

The models considered in the work differ only in the size of hard disks. We have studied models with a disk diameter $0 < d < 2\sqrt{3}a$, and, hereinafter, a is the lattice parameter. Lattice sites can be in two states: $n_i = 0$ if the site is free and $n_i = 1$ if the hard-disk center is located in this site. These models can be conveniently described in terms of the neighbor exclusions, when there is an infinitely strong repulsion between occupied sites at some distance from each other. According to this terminology, the considered models can be classified by the number of the coordination sphere: from 1NN to 5NN. We will investigate in detail only the models with restrictions up to the third neighbor. Figure 1 presents the regions corresponding to the infinitely strong repulsions in models from 1NN to 3NN and the respective hard disks. Thus, if we take into account the neighbor exclusions, then the thermodynamic Hamiltonian for all models can be defined as follows:

$$\beta H_{\text{eff}} = -\mu \sum_i n_i, \tag{1}$$

where μ is the chemical potential; i runs over all lattice site; $\beta = 1/(k_B T)$, where k_B is Boltzmann constant; and T is the absolute temperature. For simplicity, we suppose β equal to 1 and further give all the values in a dimensionless form. In addition, periodic boundary conditions were implemented in all the models.

The simplest case is the model with $d < a$, when the size of the adsorbed molecules is small compared to the distance between neighboring sites. Thus, there are no restrictions on the states of neighboring sites. This model is the well-known Langmuir adsorption model (LM). Phase behavior of such a system is not affected by the lattice geometry. As the chemical potential of the gas phase (pressure) increases, the number of molecules on the surface gradually grows, and when the chemical potential reaches a certain value, the close-packed phase $\Psi 1$ with a density of $\varphi_{\Psi 1} = 1$ is formed. It is worthwhile to note that the LM is known to have no phase transition at nonzero temperatures. The value φ is calculated as the ratio of the number of adsorbed molecules to the total number of sites in the system. Figure 2 shows the structure of the close-packed phase in the LM model.

If the size of molecules exceeds the distance between nearest-neighbor sites ($d > a$), then the nearest-neighbor (1NN), next-nearest-neighbor (2NN), and other neighboring can be prohibited in the model. Special attention should be paid to the 1NN model, which is also called the hard hexagon

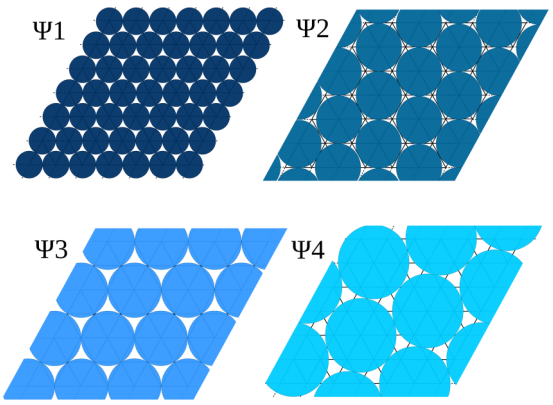

FIG. 2. Structure of the close-packed phases formed in the considered models.

model. The exact solution was proposed for it in 1980 [40,41]. This allows us to compare the accuracy of the obtained results. In all considered models only the lattice gas phase ($\varphi = 0$) is present at low values of the chemical potential. At high values, the structure becomes as dense as possible for a particular model. According to the ground-state analysis, the observed phases have the following densities: $\varphi_{\Psi 2} = 1/3$ in the 1NN model, $\varphi_{\Psi 3} = 1/4$ in the 2NN model, $\varphi_{\Psi 4} = 1/7$ in the 3NN model, $\varphi_{\Psi 5} = 1/9$ in the 4NN model, and $\varphi_{\Psi 6} = 1/12$ in the 5NN model. The close-packed structures for the first four models are shown in Fig. 2. The extreme case of the considered sequence of lattice models is a continuous model of hard disks. Recall that two phase transitions occur in the continuous model of hard disks with increase of the layer density: the first-order transition from the surface liquid to the "hexatic phase" and the continuous phase transition from the "hexatic phase" to the crystal [42]. In order to compare the data obtained for the different models in the considered set, we introduce another definition of the density: the ratio between the amount of adsorbed molecules and the capacity of the monolayer $\rho = \varphi/\varphi_{\max}$. The monolayer capacity corresponds to the maximum possible amount of the molecules in the monolayer.

III. TENSOR RENORMALIZATION GROUP AND TRANSFER-MATRIX METHODS

To study the considered models we need to calculate their partition function. It allows us to obtain the desired thermodynamic properties using the following equations:

$$Z = \sum_i e^{\beta H_i},\ \beta\Omega = -\ln(Z), \tag{2}$$

$$\varphi = -\left(\frac{\partial\Omega}{\partial\mu}\right)_T,\ S = -\left(\frac{\partial\Omega}{\partial T}\right)_\mu,\ C_V = T\left(\frac{\partial S}{\partial T}\right)_\mu, \tag{3}$$

where Z is the partition function, i is a number of microstates of the system, Ω is the grand canonical potential, S is entropy, and C_V is heat capacity. The finite-difference formulas were used for numerical differentiation. The differentiation step was $10^{-4}\ k_B$ for T and k_BT for μ.

Baxter proposed to calculate the partition function through a contraction of a tensor network consisting of a fourth-rank tensor. Each tensor describe the interactions between the four nearest lattice sites. This approach is called the interaction-round-a-face (IRF) model [43]. The transformation of a lattice model into a tensor network is schematically shown in Fig. 3. Black dots denote identity tensors (main diagonal elements are 1s and all others are 0's). The term COPY-dot was coined for these tensors in Ref. [44]. W is an interaction-round-a-face tensor, which contains information about interactions of four neighboring sites. The trace of the obtained tensor network is a partition function $Z = t\mathrm{Tr}(\otimes_{i=1}^{N} T)$.

In original paper [20] Levin and Nave proposed to use the TRG method for triangular, square, and honeycomb lattices with the nearest-neighbor interactions with specific schemes of tensor network contraction. Later TRG was adopted to various models: the classical dimers model [45], the lattice boson model [46], the O(3) model [47], and the XY model [48]. In contrast with above-mentioned models the hard-disks

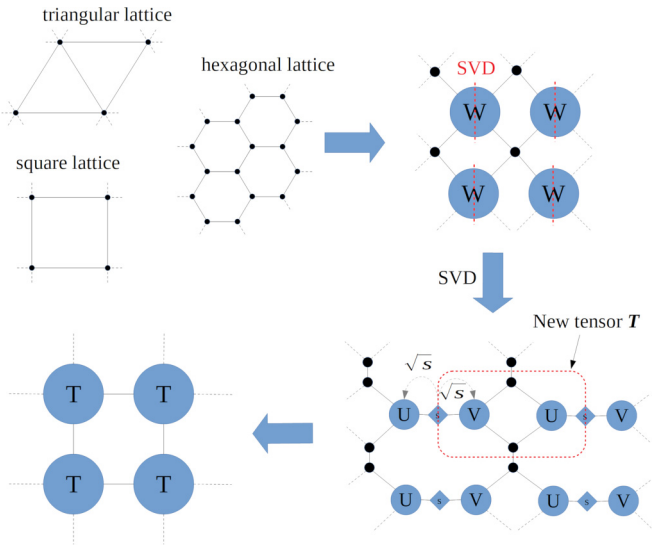

FIG. 3. Transformation of a lattice model to regular tensor network.

models include long-range interactions. It forbids straightforward usage of simple tensor network for triangular lattice.

Therefore here we have employed the Baxter's IRF approach to build tensor networks of square lattice topology for all xNN models. Long-range interactions have been taken into account via considering several neighboring sites of an original lattice as a single site. So in the refined lattice only interactions between nearest and next-nearest neighbors are presented. These interactions can be included in IRF four-legged tensor. It is important to note that this construction can be universally applied to any 2D lattice with arbitrary crystalline symmetry. It means that TRG method potentially can be applied to a wide range of physical objects in a routine way. Although specific tensor network representations can be more efficient for particular lattices and interaction Hamiltonians, simple and universal construction is crucial for wide adoption of the method.

In the considered set of the hard-core lattice models infinitely strong repulsions are arose between occupied sites (where $n_i = 1$) at a certain distance. Eliminating these excluded configurations significantly saves the computational resources. For example, merging the nearest-neighbor sites in the 1NN model results in a site with three states but not four. It follows from the fact that pair configuration, where both nearest-neighbor sites are occupied, is excluded.

Unfortunately, direct calculation of partition function for systems of large size is impossible. In this regard, various approximate methods are utilized. Here we used the TRG algorithm as implemented in the SUSMOST [49]. The idea of the approach is to reduce singular value spectrum of the tensor to a specified number D (Fig. 4). When the D decreases, it obviously leads to a growth of the computational error. It is difficult to estimate the accuracy of the calculations with this approach. However, the computational experiments on some models show that results converge to exact values when the D increases [20,26].

The transfer-matrix method used earlier for studying lattice models of hard disks can also be implemented in the

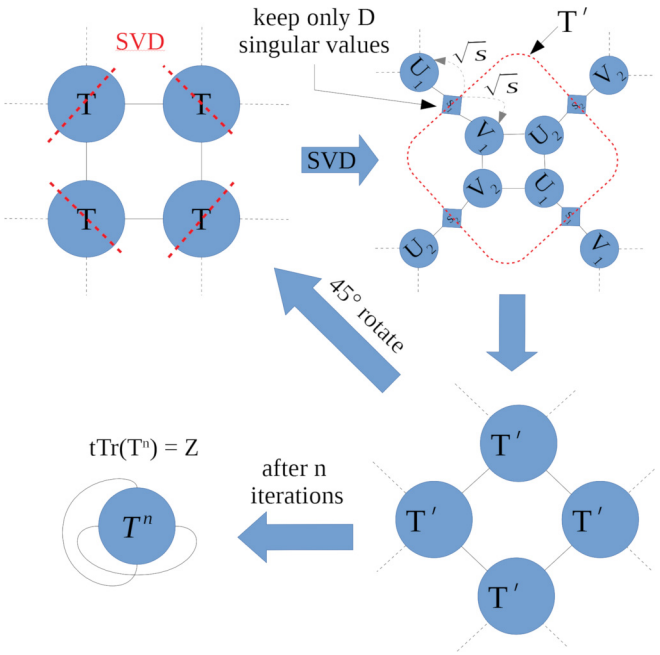

FIG. 4. Schematic representation of the TRG algorithm.

tensor form. The main concept of the method is to find the largest eigenvalue of a certain matrix that describes the interactions between M sites (rings on a semi-infinite cylinder). The resulting eigenvalue corresponds to the partition function of a system with size $M \times \infty$. Since numerical algorithms allow us to find the eigenvalue of a matrix with a predetermined accuracy, the value of the calculation error is always known in advance. The main problem of the method is the exponential growth of the calculation time with increasing M.

Algorithms for finding the largest eigenvalue are usually associated with a vector-matrix multiplication. It can also be represented in the tensor form for the general case (Fig. 5). Here the multidimensional tensor X acts as

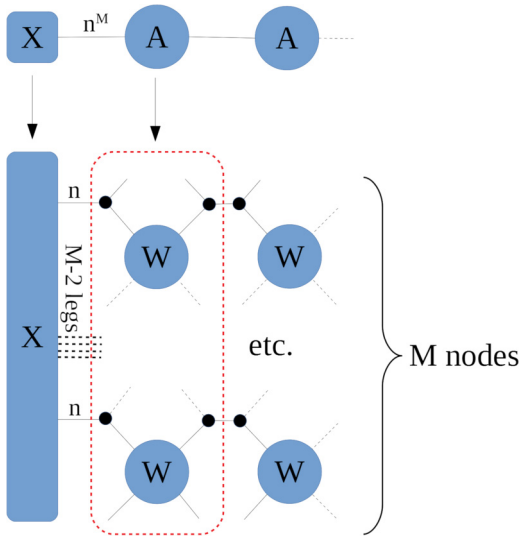

FIG. 5. Tensor representation of the transfer-matrix technique.

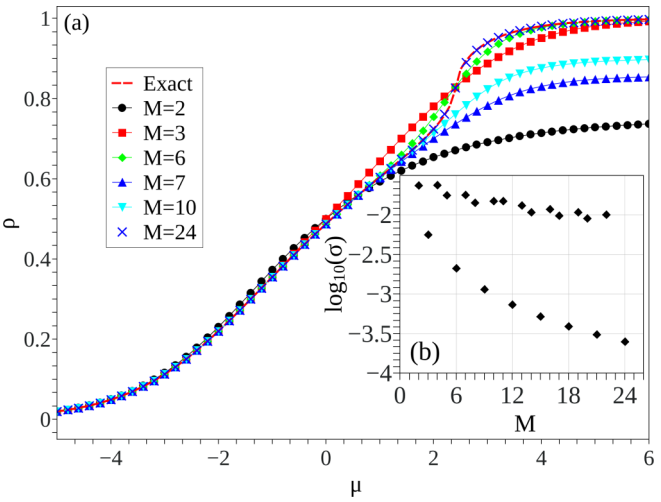

FIG. 6. Results of the TM calculations for the 1NN model: (a) Baxter's exact and calculated adsorption isotherms and (b) MAE of $\Omega_M(\mu)$ as function of M.

the left vector in a sequential contraction procedure. The transfer-matrix is represented as a set of W tensors. This approach allows us to store in memory only vector X and tensor W, which significantly reduces the amount of required RAM.

The multiplication by the right vector is carried out in a similar way. The eigenvalue was calculated using the restarted Arnoldi method. The tensors contractions were implemented as a linear operator, which was further used to find the eigenvalue using the SciPy library.

IV. RESULTS

A. 1NN model

First, we consider the results obtained by the TM method for the 1NN model. The adsorption isotherms were calculated for the systems of various sizes $M = 2$–24. The upper limit of the parameter $M = 24$ was caused by the available computing resources. The exact Baxter isotherm and isotherm calculated by the TM method are shown in Fig. 6(a).

We additionally compared a value of the grand thermodynamic potential with the exact solution [Fig. 6(b)]. The mean absolute error (MAE) σ of the M function was calculated by comparing with Baxter's exact solution and defined as follows [40,41]:

$$\sigma(M) = \frac{\sum_{\mu} |\Omega_M(\mu) - \Omega_{\text{exact}}(\mu)|}{N}, \tag{4}$$

where N is the number of points along the curve.

As seen, the behavior of the system strongly depends on the size of the semi-infinite lattice. The fact is the unit cell size of the $\Psi 2$ phase equals 3. To obtain a correct result the value of the parameter M must be a multiple of 3, that is, the smallest linear size of the phase unit cell. If several phases are formed in the system, then it is necessary to choose M multiple of the smallest unit cell among all the phases observed in the system. Therefore, it is necessary to analyze the ground state of the model before the TM calculations. As follows

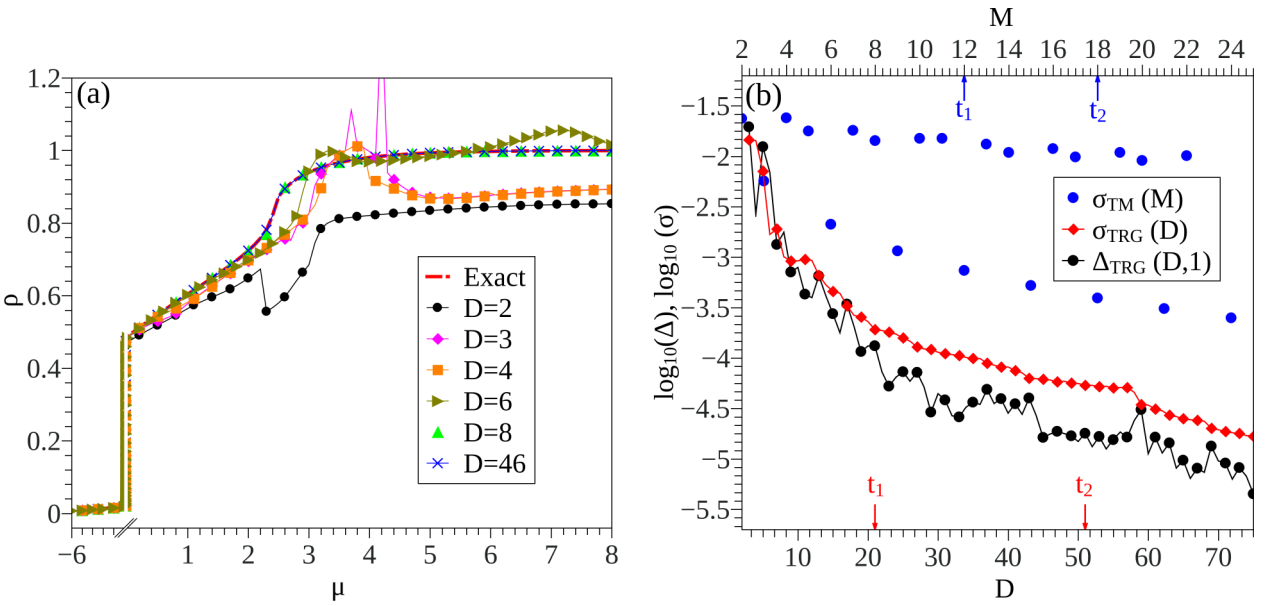

FIG. 7. Results of the TRG calculation for the 1NN model: (a) Baxter's exact and calculated adsorption isotherms and (b) the accuracy estimations of the TM and TRG calculations of the grand thermodynamic potential. The points t_1 and t_2 indicate the values of the parameters M and D corresponding to approximately the same computational times. For $M = 12$ and $D = 17$, $t_1 = 15$ s, for $M = 18$ and $D = 38$, $t_2 = 30$ min on an eight-CPU computer.

from Fig. 6(b), the accuracy of the TM calculations increases significantly, when taking into account only M multiple of 3. Thus, reliable results of the TM calculations require the maximum possible values of the M parameter and taking into account the multiplicity of the unit cells.

The corresponding isotherms were computed using the TRG method at various values of $D = 2$–46 [Fig. 7(a)]. The accuracy of the TRG calculations was estimated at $D = 2$–75 [Fig. 7(b)]. There are t_1 and t_2 points in Fig. 7(b) that provide a comparison of the time required for the calculations using TM and TRG algorithms. It can be seen that the TRG method is superior in accuracy to the TM method at a lower computational cost.

Similarly to the TM method, the increase of the D parameter (the number of kept singular values) leads to the growth of the calculation accuracy. It is seen that even at $D >= 8$ the difference is inconspicuous. Note that the TRG method does not require us to take into account the multiplicity of the parameter D to the sizes of the unit cells. This allows us to investigate the system without a preliminary analysis of the ground state. The convergence of the results was estimated by the mean absolute deviation Δ between the data obtained at different values of D:

$$\Delta(D, r) = \frac{\sum_{\mu} |\Omega_D(\mu) - \Omega_{(D-r)}(\mu)|}{N}. \qquad (5)$$

All calculations for this model were carried out at $D <= 81$. It should be mentioned that an additional reduction (by $\sqrt{D}$) was applied for each dimension of the tensor. This approach can substantially reduce the calculation time in some cases.

As can be seen in the isotherm plots, a continuous phase transition occurs in the system. According to the exact solution of Baxter [40,41], the phase-transition point in this system is $\mu_c = \ln(\frac{11+5\sqrt{5}}{2}) = 2.406059$. We have evaluated it from position of the heat capacity peak [Fig. 8(a)].

As demonstrated in Fig. 8, in the TM calculations the heat capacity peak shifts toward the exact solution with M growth. In TRG calculations displacements of the heat capacity peak is negligible at $D > 45$. For example, the phase transition at $D = 81$ appears at the chemical potential $\mu_c = 2.405992$ (error 6.7×10^{-5}), but TM at $M = 24$ gives $\mu_c = 2.399604$ (error 6.455×10^{-3}).

As is known, the formation of an ordered structure can be estimated by the stable minimum of the system entropy in a certain range of the variable parameter values. Figure 8(b) shows the entropy dependence on the chemical potential

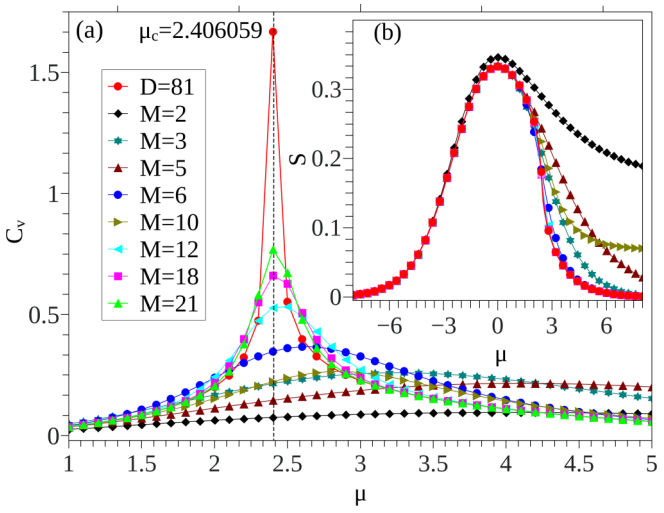

FIG. 8. Heat capacity and entropy of the 1NN model.

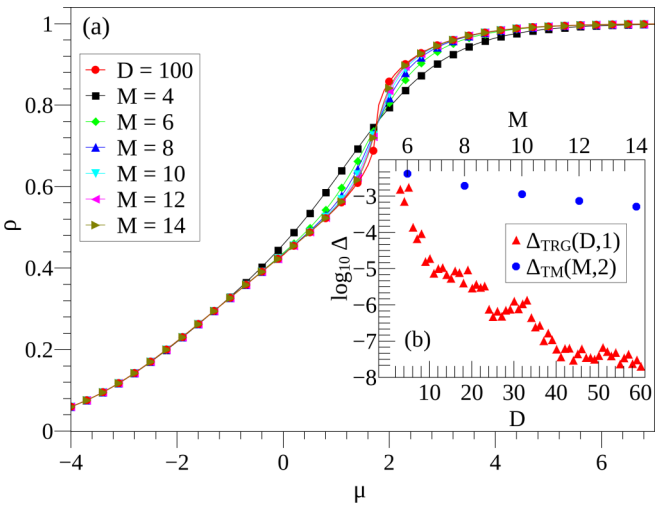

FIG. 9. Results of the TM and TRG calculations for 2NN model: (a) The adsorption isotherms and (b) the convergence of the grand thermodynamic potential.

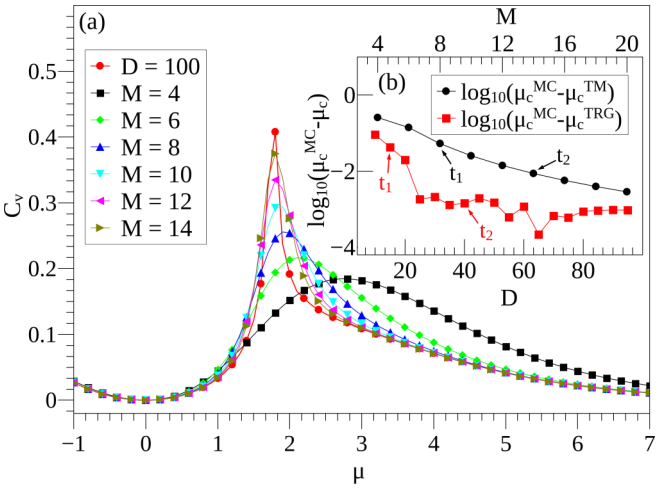

FIG. 10. Heat capacity vs. chemical potential in the 2NN model. Inset (b) illustrates the difference of the calculated μ_c with previous result [16]. The points t_1 and t_2 indicate the values of the parameters M and D corresponding to approximately the same computational times.

for the 1NN model. As can be seen, the entropy minima clearly possesses the regions of the stable lattice gas and a two-dimensional crystal. Note that the zero entropy and heat capacity in the indicated phases is a consequence of the fact that the considered model is a lattice model.

B. 2NN model

Here we consider a model with next-nearest-neighbors exclusions (2NN). Since the linear size of the unit cell of the close-packed phase equals 2, all TM calculations were carried out only for even M. Figure 9 shows the adsorption isotherms and our estimations of the calculation convergence. As can be seen in Fig. 9(a), the phase behaviors of this and previous models are similar. There is a continuous phase transition from the LG to the close-packed Ψ_2 phase. As in the case of 1NN model, a gradual change in the shape of the obtained isotherm is noticeable as the size of the system increases. Since there is no exact solution for the considered model, the convergence was estimated only by $\Delta(M, 2)$ and $\Delta(D, 1)$ parameters [Fig. 9(b)]. The maximum value of the D parameter that we used is 100, and the corresponding error is $\Delta(D = 100, r = 1) < 10^{-8}$.

The phase-transition point was determined relying on the position of the heat capacity peak [Fig. 10(a)]. To the best of our knowledge, the most accurate estimation of μ_c to today was computed by Zhang and Deng [16] with the Monte Carlo method to be 1.75682(2). Figure 10(b) shows the difference of the calculated μ_c with this estimation for different values of M and D parameters utilized in the TM and TRG methods, respectively. From the values of t_1 and t_2, one can see that for the same computation time the TRG method gives a much more accurate result. The resulting value of the critical chemical potential obtained by the TRG method is $\mu_c = 1.75587$ at $D = 100$. The TM at $M = 20$ gives the value $\mu_c = 1.75398$. It should be noted that both computation methods show the single continuous phase transition from a disordered phase with low density to the close-packed structure. This is also consistent with Monte Carlo simulations by Zhang and Deng [16].

C. 3NN model

The similar study was performed for the 3NN model. The TM calculations were conduced only for $M = 14$ and 21, since the unit cell size of the close-packed structure is 7×7. The calculated isotherms and heat capacity are presented in Fig. 11(a).

The phase transition determined by the TM technique practically does not change with increasing of M and coincides with $\mu_c = 4.4488$ obtained by the TRG method for $D = 121$. Absence of the scaling behavior indicates the first-order phase transition, setting the 3NN model apart from those considered earlier. Thus, 1NN-3NN models on triangular and square lattices behave in the qualitatively same way [7].

D. 4NN and 5NN models

For the 4NN and 5NN models the adsorption isotherms were computed only with the TRG method (Fig. 12). As shown, there is a continuous phase transition in the 4NN model and presumably the first-order phase transition in the 5NN model. For the 4NN model μ_c has been estimated to be between 2.65 and 2.7. For the 5NN model μ_c is from 4.4 to 4.5. It is interesting to note that μ_c for 5NN is close to μ_c for 3NN.

It is remarkable that a continuous phase transition was initially assumed for the 4NN model on a square lattice [7]. However, it was found that two different phase transitions occur [8]. In the case of a triangular lattice we observed a single continuous, yet rapid, phase transition. Coverage changes rather fast in the vicinity of μ_c, so we had to conduct computations with very small step by μ to conclude about type of the transition. In order to determine the presence of a second phase transition, additional studies are required. Here we can only claim that at least one phase transition occurs

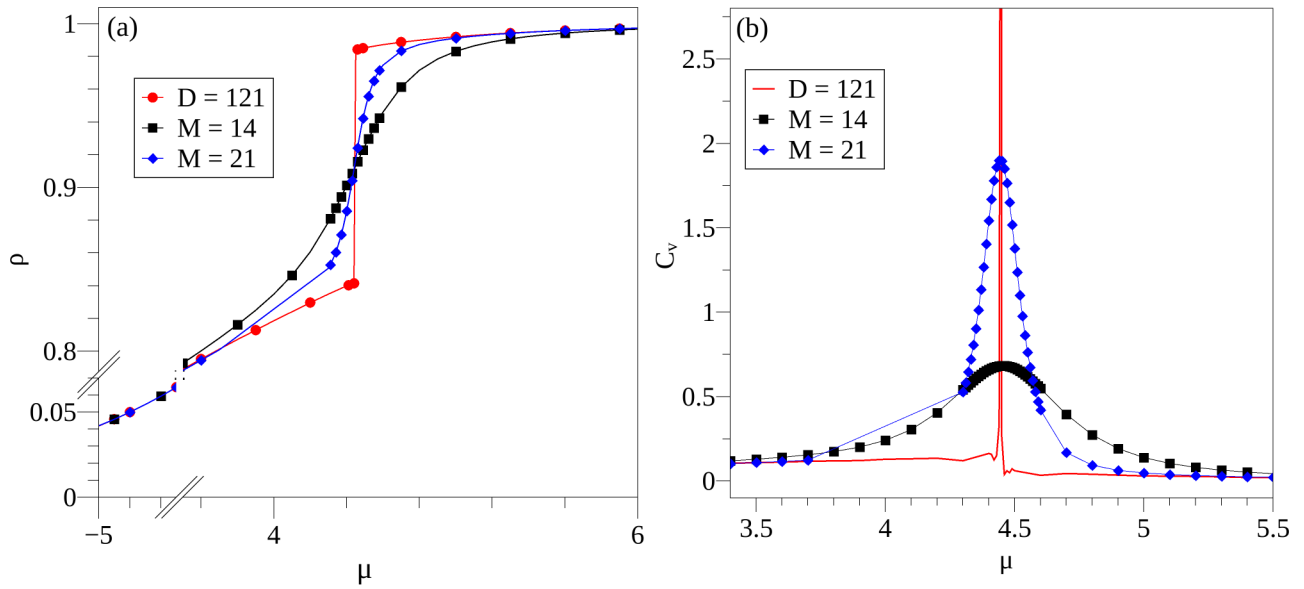

FIG. 11. Density (a) and heat capacity (b) dependence on chemical potential in the 3NN model.

in this system. In the 5NN model we observed the first-order phase transition that corresponds to the square-lattice case [7].

Figure 12 also shows the adsorption isotherms calculated with Langmuir, Volmer, and the continuous hard-disk models. One can see that the phase transitions in the considered models occur in the region between the Langmuir model and the continuous models. A further increase in the disk size is expected to gradually shift the phase-transition point toward higher μ values. Further study of the 4NN and 5NN models, as well as more complex models, is planned in the future, since this requires calculations for $D > 150$ and/or the use of modified versions of tensor network algorithms.

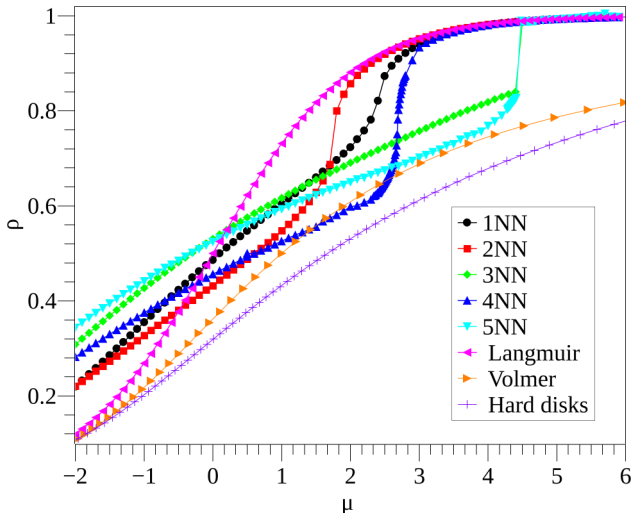

FIG. 12. The adsorption isotherms of all considered models compared with the Langmuir, Volmer, and continuous hard-disk models [39].

V. CONCLUSION

In this paper we have studied the thermodynamic characteristics of the hard-disk models on a triangular lattice, using transfer-matrix and tensor renormalization group methods. The models differ by the diameter of the disks from a to $2\sqrt{3}a$, where a is the lattice constant. We have proposed a universal construction of the uniform square tensor network for the TRG method. It simplifies the implementation of tensor-network algorithms for lattices of different symmetry. Using the TRG and TM methods we have calculated heat capacity and layer density as functions of chemical potential. Superiority of TRG over TM in terms of accuracy and performance was observed for the considered models. An important virtue of the TRG method is the intrinsic infinity of the simulated system, which makes it unnecessary to do a ground-state analysis beforehand.

Critical values of chemical potential have been computed for all considered models. For the 1NN model both the TRG and TM methods exhibited good accuracy compared with the exact solution. For the 2NN model, TRG and TM produced consistent estimations of μ_c. To the best of our knowledge, estimations of μ_c for the 3NN, 4NN, and 5NN models have been computed for the first time here. The 3NN and 5NN models shows the first-order phase transition, and the 4NN model shows a continuous yet rapid phase transition. Generally, types of phase transitions in the considered sequence of models are similar to ones of corresponding models on square lattice. Obtained adsorption isotherms of the considered models in the vicinity of phase transitions appeared to be intermediate between Langmuir and continuous Volmer and hard-disks isotherms, which is consistent with general theoretical reasoning.

ACKNOWLEDGMENTS

This study was supported by the Russian Science Foundation under Grant No. 17-71-20053.

[1] A. Ibenskas, M. Šimėnas, and E. E. Tornau, Numerical engineering of molecular self-assemblies in a binary system of trimesic and benzenetribenzoic acids, J. Phys. Chem. C **120**, 6669 (2016).

[2] A. Ibenskas, M. Šimėnas, and E. E. Tornau, Multiorientation model for planar ordering of trimesic acid molecules, J. Phys. Chem. C **122**, 7344 (2018).

[3] P. Szabelski, D. Nieckarz, and W. Rżysko, Structure formation in 2d assemblies comprising functional tripod molecules with reduced symmetry, J. Phys. Chem. C **121**, 25104 (2017).

[4] P. Szabelski, W. Rżysko, and D. Nieckarz, Directing the self-assembly of tripod molecules on solid surfaces: A Monte Carlo simulation approach, J. Phys. Chem. C **120**, 13139 (2016).

[5] A. Kasperski and P. Szabelski, Theoretical modeling of the formation of chiral molecular patterns in self-assembled overlayers, Sur. Sci. **629**, 57 (2014).

[6] V. A. Gorbunov, S. S. Akimenko, and A. V. Myshlyavtsev, Cross-impact of surface and interaction anisotropy in the self-assembly of organic adsorption monolayers: a monte carlo and transfer-matrix study, Phys. Chem. Chem. Phys. **19**, 17111 (2017).

[7] H. C. M. Fernandes, J. J. Arenzon, and Y. Levin, Monte Carlo simulations of two-dimensional hard core lattice gases, J. Chem. Phys. **126**, 114508 (2007).

[8] T. Nath and R. Rajesh, Multiple phase transitions in extended hard-core lattice gas models in two dimensions, Phys. Rev. E **90**, 012120 (2014).

[9] M. Šimėnas and E. E. Tornau, Pin-wheel hexagons: A model for anthraquinone ordering on Cu (111), J. Chem. Phys. **139**, 154711 (2013).

[10] D. Nieckarz and P. Szabelski, Understanding pattern formation in 2D metal-organic coordination systems on solid surfaces, J. Phys. Chem. C **117**, 11229 (2013).

[11] S. S. Akimenko, V. A. Gorbunov, A. V. Myshlyavtsev, and P. V. Stishenko, Generalized lattice-gas model for adsorption of functional organic molecules in terms of pair directional interactions, Phys. Rev. E **93**, 062804 (2016).

[12] A. V. Myshlyavtsev and P. V. Stishenko, Potential of lateral interactions of CO on Pt (111) fitted to recent STM images, Sur. Sci. **642**, 51 (2015).

[13] X. Feng, H. W. J. Blöte, and B. Nienhuis, Lattice gas with nearest-and next-to-nearest-neighbor exclusion, Phys. Rev. E **83**, 061153 (2011).

[14] W. Guo and H. W. J. Blöte, Finite-size analysis of the hard-square lattice gas, Phys. Rev. E **66**, 046140 (2002).

[15] A. Ibenskas, M. Šimėnas, and E. E. Tornau, Antiferromagnetic triangular Blume-Capel model with hard-core exclusions, Phys. Rev. E **89**, 052144 (2014).

[16] W. Zhang and Y. Deng, Monte Carlo study of the triangular lattice gas with first- and second-neighbor exclusions, Phys. Rev. E **78**, 031103 (2008).

[17] W. Krauth, *Statistical Mechanics: Algorithms and Computations*, Oxford Master Series in Physics (Oxford University Press, Oxford, 2006).

[18] D. P. Landau and K. Binder, *A Guide to Monte Carlo Simulations in Statistical Physics*, 4th ed. (Cambridge University Press, Cambridge, 2014).

[19] S. S. Akimenko, V. F. Fefelov, A. V. Myshlyavtsev, and P. V. Stishenko, Remnants of the devil's staircase of phase transitions in the model of dimer adsorption at nonzero temperature, Phys. Rev. B **97**, 085408 (2018).

[20] M. Levin and C. P. Nave, Tensor Renormalization Group Approach to Two-Dimensional Classical Lattice Models, Phys. Rev. Lett. **99**, 120601 (2007).

[21] S. R. White, Density Matrix Formulation for Quantum Renormalization Groups, Phys. Rev. Lett. **69**, 2863 (1992).

[22] P. Czarnik, M. M. Rams, and J. Dziarmaga, Variational tensor network renormalization in imaginary time: Benchmark results in the Hubbard model at finite temperature, Phys. Rev. B **94**, 235142 (2016).

[23] A. Kshetrimayum, H. Weimer, and R. Orús, A simple tensor network algorithm for two-dimensional steady states, Nat. Commun. **8**, 1291 (2017).

[24] L. Kohn, F. Tschirsich, M. Keck, M. B. Plenio, D. Tamascelli, and S. Montangero, Probabilistic low-rank factorization accelerates tensor network simulations of critical quantum many-body ground states, Phys. Rev. E **97**, 013301 (2018).

[25] Z. Y. Xie, J. Chen, M. P. Qin, J. W. Zhu, L. P. Yang, and T. Xiang, Coarse-graining renormalization by higher-order singular value decomposition, Phys. Rev. B **86**, 045139 (2012).

[26] M. Hauru, C. Delcamp, and S. Mizera, Renormalization of tensor networks using graph-independent local truncations, Phys. Rev. B **97**, 045111 (2018).

[27] S. S. Jahromi, R. Orús, M. Kargarian, and A. Langari, Infinite projected entangled-pair state algorithm for ruby and triangle-honeycomb lattices, Phys. Rev. B **97**, 115161 (2018).

[28] H. H. Zhao, Z. Y. Xie, Q. N. Chen, Z. C. Wei, J. W. Cai, and T. Xiang, Second renormalization of tensor-network states, Phys. Rev. B **81**, 174411 (2010).

[29] G. Evenbly, Algorithms for tensor network renormalization, Phys. Rev. B **95**, 045117 (2017).

[30] G. Evenbly and G. Vidal, Tensor Network Renormalization, Phys. Rev. Lett. **115**, 180405 (2015).

[31] T. Yokoyama, S. Yokoyama, T. Kamikado, and S. Mashiko, Nonplanar adsorption and orientational ordering of porphyrin molecules on Au(111), J. Chem. Phys. **115**, 3814 (2001).

[32] T. Lelaidier, T. Leoni, A. Ranguis, A. D'Aléo, F. Fages, and C. Becker, Adsorption and growth of bis-pyrene molecular layers on Au(111) studied by STM, J. Phys. Chem. C **121**, 7214 (2017).

[33] Y. Gurdal, J. Hutter, and M. Iannuzzi, Insight into (co)pyrphyrin adsorption on Au(111): Effects of herringbone reconstruction and dynamics of metalation, J. Phys. Chem. C **121**, 11416 (2017).

[34] Y. Y. Tarasevich, V. V. Laptev, N. V. Vygornitskii, and N. I. Lebovka, Impact of defects on percolation in random sequential adsorption of linear *k*-mers on square lattices, Phys. Rev. E **91**, 012109 (2015).

[35] Y. Y. Tarasevich, N. I. Lebovka, and V. V. Laptev, Percolation of linear *k*-mers on a square lattice: From isotropic through partially ordered to completely aligned states, Phys. Rev. E **86**, 061116 (2012).

[36] P. M. Centres and A. J. Ramirez-Pastor, Percolation and jamming in random sequential adsorption of linear *k*-mers on square lattices with the presence of impurities, J. Stat. Mech.: Theory and Expe. (2015) P10011.

[37] M. G. Slutskii, L. Y. Barash, and Y. Y. Tarasevich, Percolation and jamming of random sequential adsorption samples of large

linear *k*-mers on a square lattice, Phys. Rev. E **98**, 062130 (2018).

[38] E. J. Perino, D. A. Matoz-Fernandez, P. M. Pasinetti, and A. J. Ramirez-Pastor, Jamming and percolation in random sequential adsorption of straight rigid rods on a two-dimensional triangular lattice, J. Stat. Mech.: Theory Exp. (2017) 073206.

[39] D. Henderson, A simple equation of state for hard discs, Mol. Phys. **30**, 971 (1975).

[40] R. J. Baxter, Hard hexagons: Exact solution, J. Phys. A: Math. Gen. **13**, L61 (1980).

[41] S. S. Akimenko, Python implementation of the exact solution for hard-hexagon model (2019), https://github.com/IakOBiaN/hard-hexagon.

[42] E. P. Bernard and W. Krauth, Two-Step Melting in Two Dimensions: First-Order Liquid-Hexatic Transition, Phys. Rev. Lett. **107**, 155704 (2011).

[43] R. J. Baxter, *Exactly Solved Models in Statistical Mechanics* (Academic Press Limited, London, 1982).

[44] J. D. Biamonte, S. R. Clark, and D. Jaksch, Categorical tensor network states, AIP Adv. **1**, 042172 (2011).

[45] K. Roychowdhury and C.-Y. Huang, Tensor renormalization group approach to classical dimer models, Phys. Rev. B **91**, 205418 (2015).

[46] Y. Shimizu, Tensor renormalization group approach to a lattice boson model, Mod. Phys. Lett. A **27**, 1250035 (2012).

[47] J. Unmuth-Yockey, Y. Meurice, J. Osborn, and H. Zou, Tensor renormalization group study of the 2d O(3) model, arXiv:1411.4213 (2014).

[48] J. F. Yu, Z. Y. Xie, Y. Meurice, Y. Liu, A. Denbleyker, H. Zou, M. P. Qin, J. Chen, and T. Xiang, Tensor renormalization group study of classical *XY* model on the square lattice, Phys. Rev. E **89**, 013308 (2014).

[49] S. S. Akimenko, G. D. Anisimova, A. I. Fadeeva, V. F. Fefelov, V. A. Gorbunov, T. R. Kayumova, A. V. Myshlyavtsev, M. D. Myshlyavtseva, and P. V. Stishenko, SUSMOST: Surface science modeling and simulation toolkit (2017), http://susmost.com.